On the influence of boundary conditions when determining transport coefficients from digital images of porous media

J Shi, G Boyer, V. Mourzenko, Jean-François Thovert

On the influence of boundary conditions when determining transport coefficients from digital images of porous media.

J. Shi[a,b], G. Boyer[a], V.V. Mourzenko[b], J.-F. Thovert[b]

[a] *PSN-RES, SA2I, Institut de Radioprotection et de Sûreté Nucléaire (IRSN), Cadarache, France.*
[b] *Institut Pprime, CNRS, Chasseneuil du Poitou, France.*

Keywords: Thermal conductivity, Boundary conditions, Digital images, Tomography

The increasing access to 3d digital images of porous media provides an ideal avenue for the determination of their transport properties, by solving the governing equations in their actual microscale geometry and evaluating the tensor coefficient that relates the mean flux and driving gradient, without resorting to any a priori modelling or morphological hypotheses. However, the first and puzzling question along the way is the choice of the conditions to be imposed for this resolution at the boundaries of the necessarily finite sample (see *e.g.*, [1, 2]). When faced with this question for the practical evaluation from a tomographic image of the thermal conductivity of a porous material [3], we took the opportunity to explore this methodological issue in more details with the purpose of:

- quantifying the influence of the boundary conditions, in relation with the parameters of the system (porosity, characteristic length scale of the microstructure, ratio of the two phases conductivities);
- assessing the expected accuracy and the level of confidence associated with the predictions;
- if possible, devising an approach including criteria for the detection of the risk of serious artifacts.

To this end, a study is underway with a systematic sweep of the parameters. Synthetic media are examined, generated from a Boolean sphere model or from thresholded, spatially correlated Gaussian fields. Various kinds of boundary conditions (B.C.) and treatments are considered. Note that the material considered in our application is expected for physical reasons to be anisotropic. This precludes periodization by symmetrization or imposing a no-flux condition at the transverse sample boundaries, since such techniques can only result in eigenvectors aligned with the computation directions.

The work is in progress at the time of writing and the build-up of a comprehensive data set is still under completion. Applications to tomographic images of various real material will also be performed.

Only an illustrative example is presented here. The sample was generated by thresholding a Gausian field, with a porosity ϵ=0.12 and an isotropic, negative exponential spatial correlation function, with a decay length l_e taken as the length unit. The $[128 l_e]^3$ sample is periodic, but a $[124 l_e]^3$ (aperiodic) block Ω was extracted from it. The pore-filling fluid as a unit conductivity ($\lambda_p = 1$) and the solid is much less conducting ($\lambda_s = 10^{-4}$). Laplace's equation is solved in Ω with uniform Dirichlet conditions at the upstream and downstream boundaries (successively along the $x-$, $y-$ and $z-$axes), or with periodic conditions with a mean gradient corresponding to the same drop ΔT.

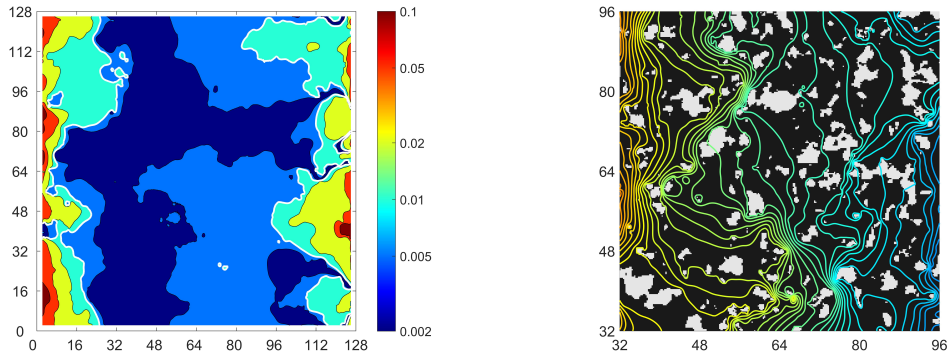

Figure 1: $|T_P - T_D| / \Delta T$ in a mid-section through the sample (left) and isothermal contours in a central part (right).

These two procedures yield temperature fields T_D and T_P, respectively, and estimates $\mathbf{\Lambda}_D$ and $\mathbf{\Lambda}_P$ of the conductivity tensor. The two fields are compared in Fig. 1, in a median cross-section parallel to the flow direction (here along the $x-$axis). The differences induced by the different B.C. extend over a distance much larger than the characteristic microscale. They drop below $\Delta T/100$ only beyond a distance about $32l_e$ from the left and right boundaries. Organization over a length so much larger than the textural scale probably results from the relative proximity to the percolation threshold ($\epsilon_c \sim 0.09$). The conductivity estimates also differ significantly, by 8 to 12% along x, y and z (Fig. 2a).

It can be expected that a central region exists, where the mean flux $\langle \boldsymbol{q} \rangle$ and gradient $\langle \nabla T \rangle$ are related by a constant conductivity tensor, irrespective of the "far-field" conditions that induce $\langle \nabla T \rangle$, thereby providing an intrinsic measure of $\mathbf{\Lambda}$. This was checked by peeling a peripheral layer M from Ω, leaving a $[124l_e$ -$2M]^3$ sub-domain Ω_c, where $\langle \boldsymbol{q} \rangle_c$ and $\langle \nabla T \rangle_c$ were measured. From the data for the gradient along x, y and z and for the two B.C.'s, two estimates $\mathbf{\Lambda}_{D,c}(M)$ and $\mathbf{\Lambda}_{P,c}(M)$ can be obtained. Figure 2a confirms that their diagonal components indeed converge within about $\pm 1.5\%$ when $M \geq 16l_e$.

Yet, are they a reliable prediction of an unambiguous effective tensor $\mathbf{\Lambda}$? Note first that $\mathbf{\Lambda}_{D,c}$ and $\mathbf{\Lambda}_{P,c}$ are constant and in agreement in a plateau $18l_e \lesssim M \lesssim 34l_e$ (Fig. 2b) , which is fine, but smaller by about 7% than a clean reference value obtained in the initial $[128l_e]^3$ periodic sample with periodic B.C.. The very mild porosity variations (except in very small Ω_c when $M > 40l_e$) cannot explain this difference. Then recall that $\mathbf{\Lambda}$ should be symmetric. A relative measure of assymetry can be defined as

$$\mathcal{A}'(\mathbf{\Lambda}) = \mathcal{A}(\mathbf{\Lambda})/\overline{\Lambda}\,, \qquad \text{with} \quad \mathcal{A}^2(\mathbf{\Lambda}) = \sum_{i \neq j} \left[(\Lambda_{ij} - \Lambda_{ji})/2\right]^2 \qquad \text{and} \quad \overline{\Lambda} = \frac{1}{3}\sum_i \Lambda_{ii} \tag{1}$$

$\mathcal{A}'(\mathbf{\Lambda}_{D,c})$ and $\mathcal{A}'(\mathbf{\Lambda}_{P,c})$ are plotted in Fig. 2c and found to be very similar as soon as $M \gtrsim 10l_e$. However, they can reach 5% in the interval $18l_e \lesssim M \lesssim 34l_e$. A measure of the difference of two tensors $\mathbf{\Lambda}_1$ and $\mathbf{\Lambda}_2$ can also be defined from the maximal deviation $\|\boldsymbol{q}_1 - \boldsymbol{q}_2\|$ of their flux predictions, which reads

$$\mathcal{D}'(\mathbf{\Lambda}_1, \mathbf{\Lambda}_2) = \mathcal{D}/\sqrt{\overline{\Lambda_1}\;\overline{\Lambda_2}}\,, \qquad \text{with} \quad \mathcal{D}^2 = \text{largest eigenvalue of } \left[(\mathbf{\Lambda}_1 - \mathbf{\Lambda}_2)^t \cdot (\mathbf{\Lambda}_1 - \mathbf{\Lambda}_2)\right] \tag{2}$$

$\mathcal{D}'(\mathbf{\Lambda}_{P,c}, \mathbf{\Lambda}_{D,c})$ is indeed very small when $18l_e \lesssim M \lesssim 34l_e$ (Fig. 2c). However, since both $\mathbf{\Lambda}_{P,c}$ and $\mathbf{\Lambda}_{D,c}$ are assymetric, the deviation $\mathcal{D}'(\mathbf{\Lambda}_{P,c}, \mathbf{\Lambda})$ or $\mathcal{D}'(\mathbf{\Lambda}_{D,c}, \mathbf{\Lambda})$ from any possible intrinsic (and therefore symmetric) $\mathbf{\Lambda}$ is possibly much greater, and *at least* equal to $\mathcal{A}'(\mathbf{\Lambda}_{D,c})$ or $\mathcal{A}'(\mathbf{\Lambda}_{P,c})$. Hence, the agreement of $\mathbf{\Lambda}_{D,c}$ and $\mathbf{\Lambda}_{P,c}$ does not prove that they are both correct, but only that they are equally wrong.

The observations in the foregoing raise more questions, about methodological issues and physical features such as the unexpected range of the boundary disturbances, than they provide answers. These questions are currently addressed, and the systematic analysis of an extensive data set will hopefully provide the answers.

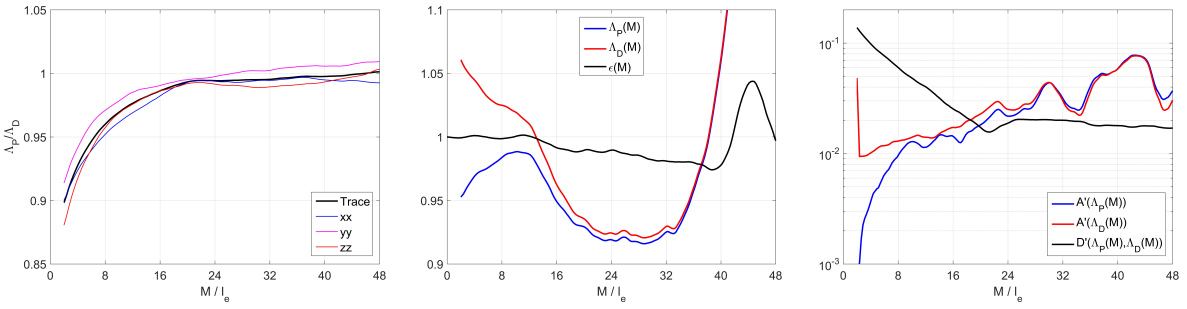

(a) (b) (c)

Figure 2: (a) Ratio $\Lambda_{P,c}/\Lambda_{D,c}$ in a central sub-domain as a function of M/l_e; (b) Traces of $\mathbf{\Lambda}_{P,c}$ and $\mathbf{\Lambda}_{D,c}$ and porosity ϵ_c measured in Ω_c, normalized by their values in the initial $[128l_e]^3$ periodic sample; (c) assymetries $\mathcal{A}'(\mathbf{\Lambda}_{D,c})$, $\mathcal{A}'(\mathbf{\Lambda}_{P,c})$ and maximal deviation $\mathcal{D}'(\mathbf{\Lambda}_{P,c}, \mathbf{\Lambda}_{D,c})$.

References

[1] Spanne P., J.-F. Thovert, C.J. Jacquin, W.B. Lindquist, K.W. Jones & P.M. Adler, Synchrotron computed microtomography of porous media. Topology and transports, Phys. Rev. Lett., **73**, 2001-2004 (1994).

[2] Guibert R., P. Horgue, G. Debenest & M. Quintard, A Comparison of Various Methods for the Numerical Evaluation of Porous Media Permeability Tensors from Pore-Scale Geometry, Math Geosci, **48**, 329-347 (2016).

[3] Shi J., G. Boyer & J.-F. Thovert, Simulation of the pyrolysis of charring polymers: influence of the porous media properties, JEMP 2018, Nantes (2018).